A copper silicide nanofoam current collector for directly grown Si nanowire network and their application as lithium-ion anodes

Ibrahim Saana Aminu, HUGH GEANEY, Sumair Imtiaz, Temilade Esther Adegoke, Nilotpal Kapuria, Gearoid A. Collins, KEVIN M. RYAN

Publication date

01-01-2020

Published in

Advanced Functional Materials;30 (38)

A Copper Silicide Nanofoam Current Collector for Directly Grown Si Nanowire Network and their Application as Lithium-ion Anodes

*Ibrahim Saana Aminu, Hugh Geaney, Sumair Imtiaz, Temilade E. Adegoke, Nilotpal Kapuria, Gearoid A. Collins, Kevin M. Ryan**

Bernal Institute, University of Limerick, Limerick V94 T9PX, Ireland

Department of Chemical Sciences, University of Limerick, Limerick V94 T9PX, Ireland

*Corresponding Author: E-mail: kevin.m.ryan@ul.ie, Phone: +353-61 213167

Materials and reagents:

All materials and chemical reagents were acquired from various reliable sources and used as supplied. Phenylsilane (~97.0%) was acquired from Fluorochem and stored in Ar-filled glovebox until used. Squalane (≥ 98%) and $LiBH_4$ (2M in tetrahydrofuran) were both supplied by Sigma-Aldrich. All metal (Al, Bi, Cu, In, Mn, Ni, Sb and Zn: ~99.999%) used as catalyst seed were obtained from Kurt J. Lesker, USA, and the high-purity planar Cu-foils (~99.9%) and Cu-foam were supplied by Pi-Kem Ltd.

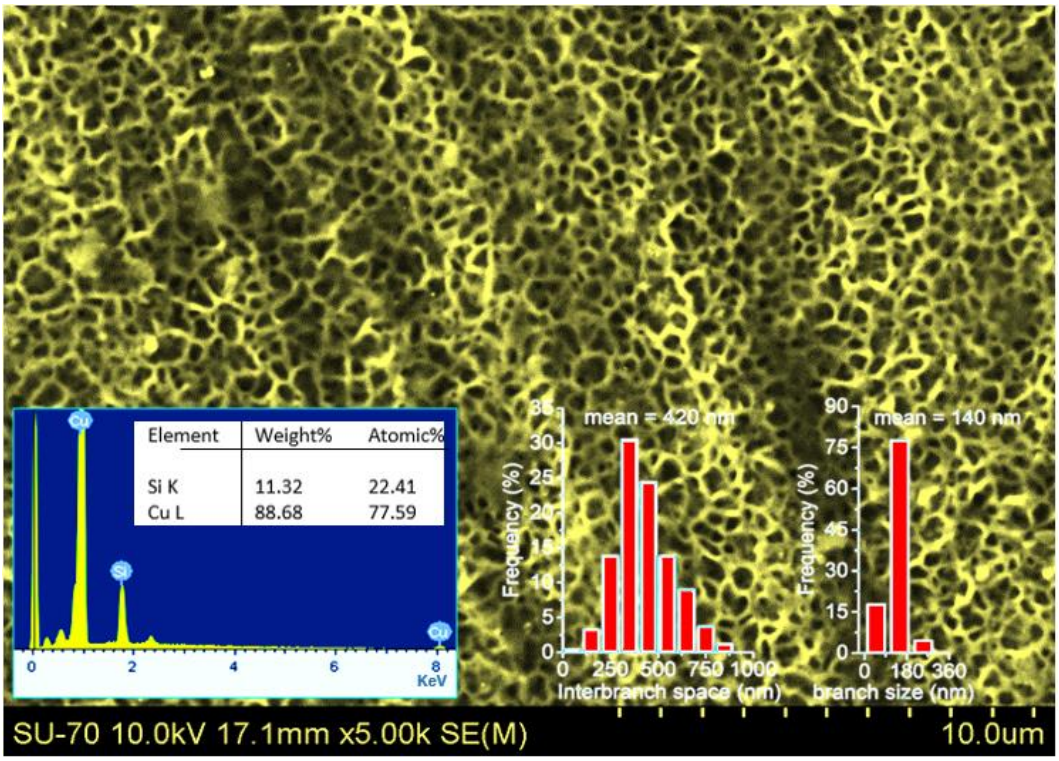

Figure S1 Low magnification SEM image of as grown 3D Cu_xSi_y NF (in false colour). Insets are EDX analysis (left), inter-branch void size (middle) and branch size (right).

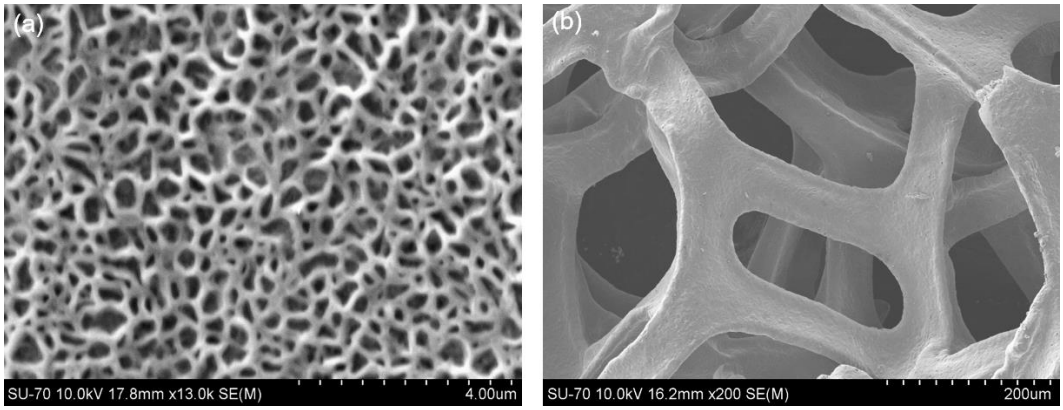

Figure S2 SEM images of (a) 3D Cu_xSi_y NF compared to (b) commercial Cu-foam. The metallic Cu-foam branch size is 457 times lager than that of the 3D Cu_xSi_y NF.

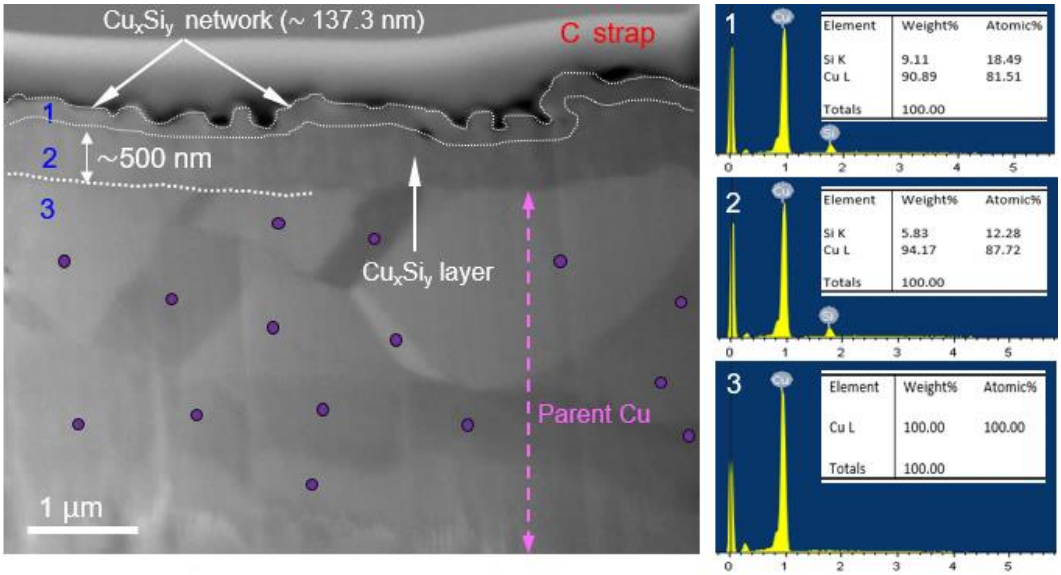

Figure S3 FIB-SEM cross-sectional image and sectional EDX analysis (numbered 1–3) of the 3D Cu_xSi_y NF. The deep FIB milling reveals clearly defined grains/boundaries in the Cu body (purple dots). It is likely that this interfacial Cu_xSi_y layer could be accountable for suppressing Cu-grain growth and/or the formation of large Cu/Si grains/compounds during Si NW growth as observed on planar Cu-foil.

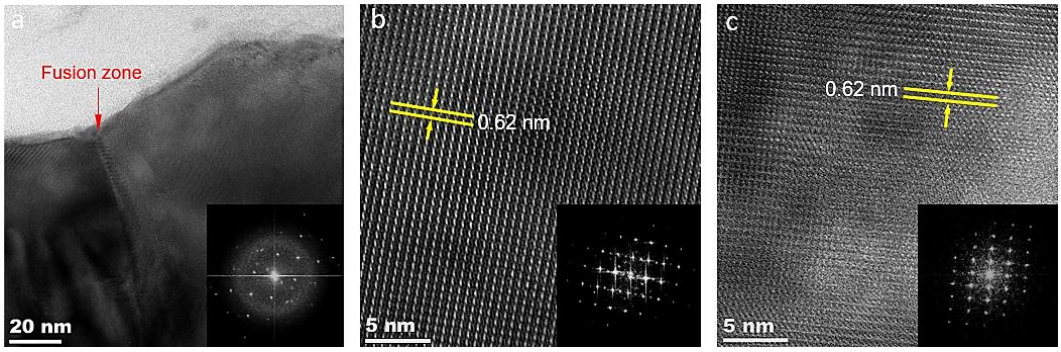

Figure S4 TEM images of (a) low magnification of the 3D Cu_xSi_y network branch, showing interparticle fusion, and high magnification of the (b) network branch and (c) silicide layer at the interface as indicated in Figure S3. An inset is the fast Fourier transform diffraction patterns.

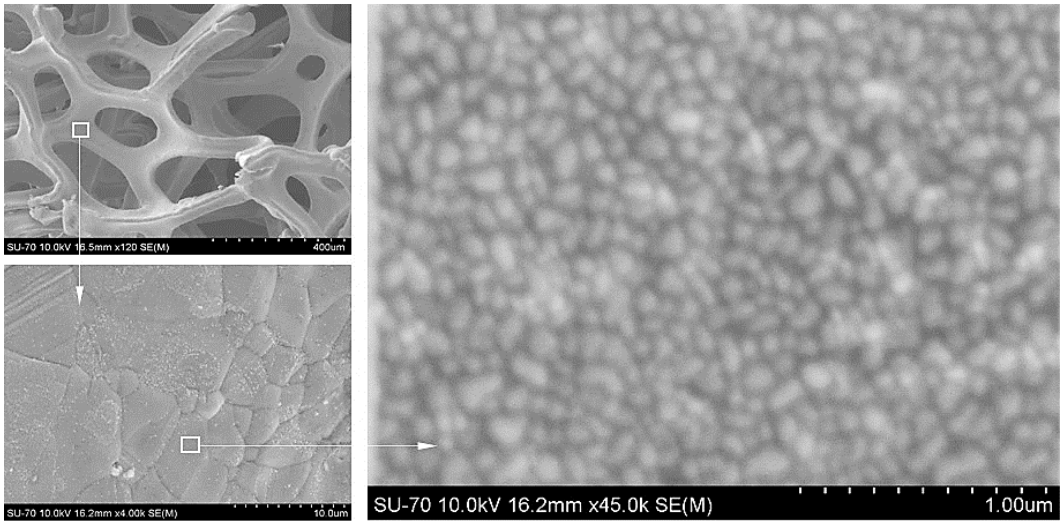

Figure S5 SEM images of Sn-seed coated Cu-foam with an average seed size of ~72 nm.

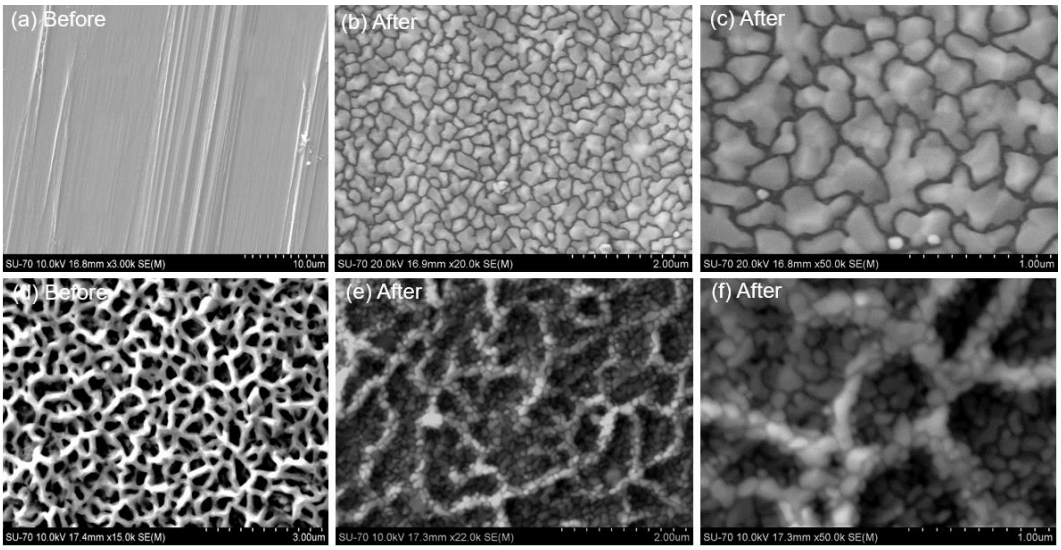

Figure S6 SEM images of (a) bare Cu-foil, (b, c) Sn-seed coated planar Cu-foil in comparison with (e) bare 3D Cu_xSi_y NF and (f, g) Sn-seed coated 3D Cu_xSi_y NF.

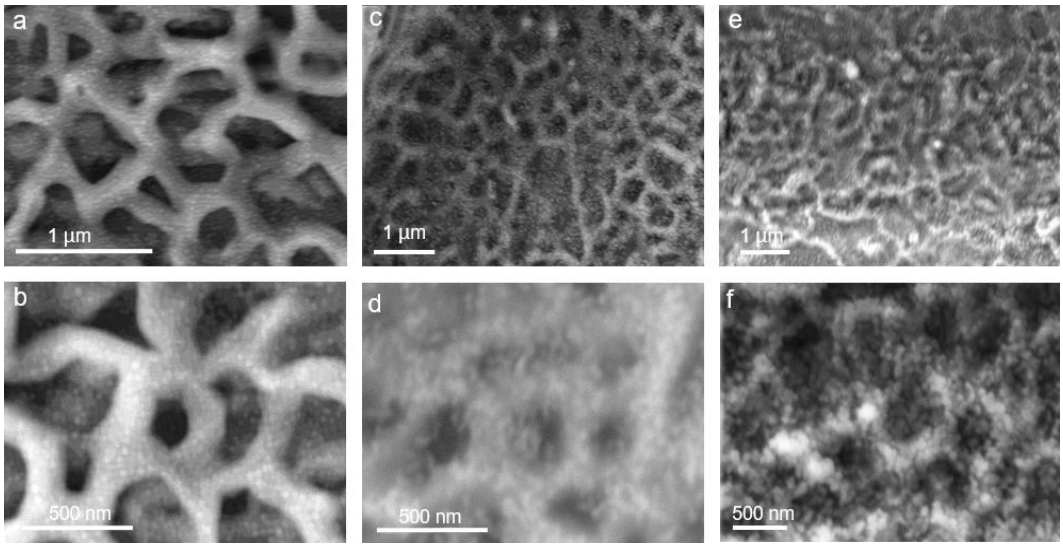

Figure S7 SEM images of (a, b) Al-seeds (~22 nm), (c, d) Zn-seeds (~34 nm) and (e, f) In-seed (~40 nm) coated 3D Cu_xSi_y NF.

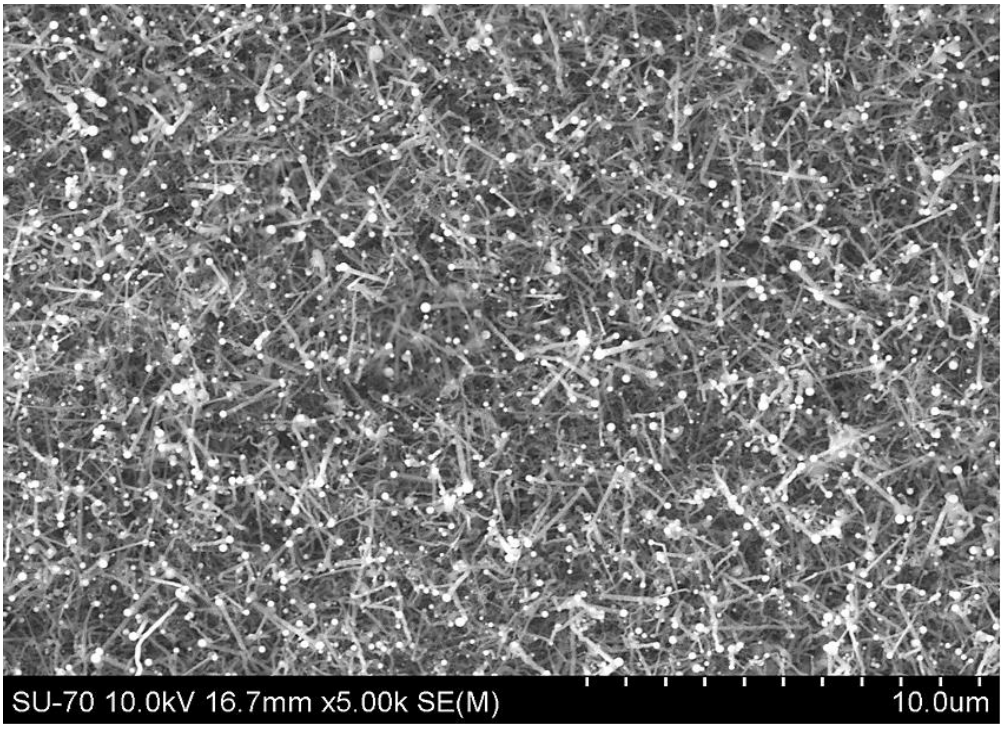

Figure S8 Low magnification SEM image of high density Si NWs grown on the 3D Cu_xSi_y NF.

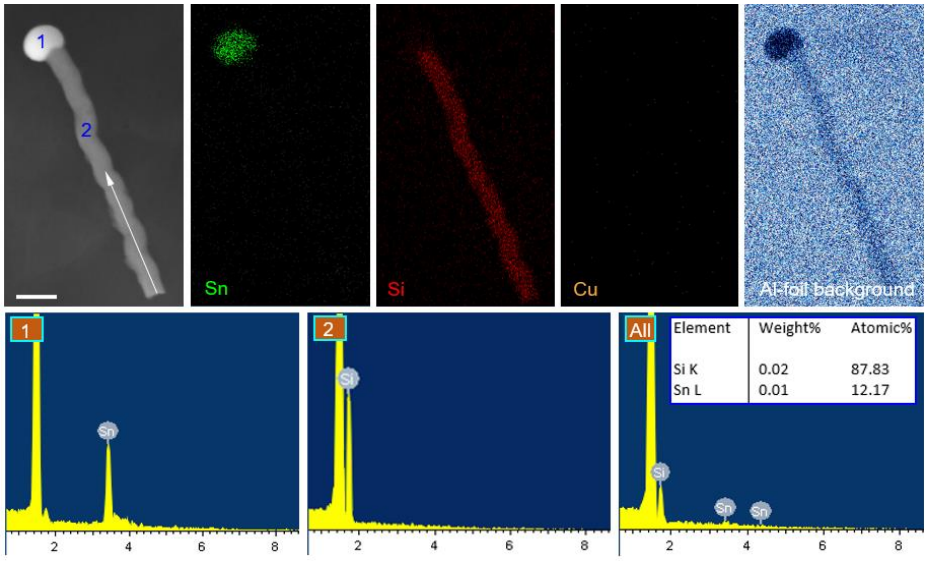

Figure S9 Mapping of element distribution and EDX analysis of Sn-seeded Si NWs scrapped on to an Al-foil for scanning, (scale: 200 nm). No Cu was detected in the Si NW body or the Sn seed.

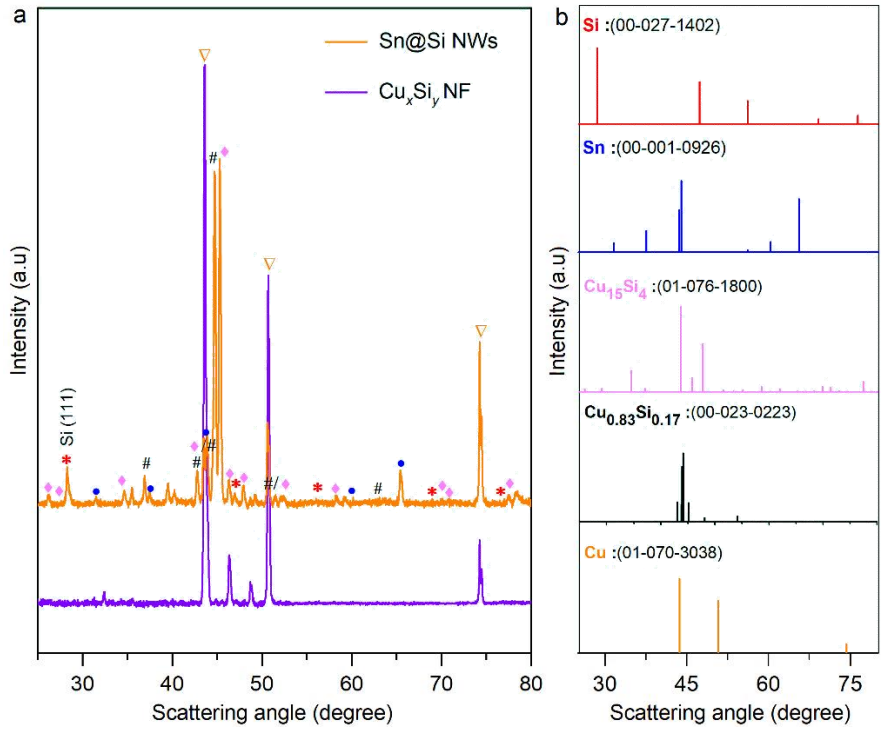

Figure S10 (a) X-ray diffraction pattern of the bare 3D Cu_xSi_y NF and Sn-seeded Si NWs on the 3D Cu_xSi_y NF and (b) corresponding reference patterns and JCPDS codes.

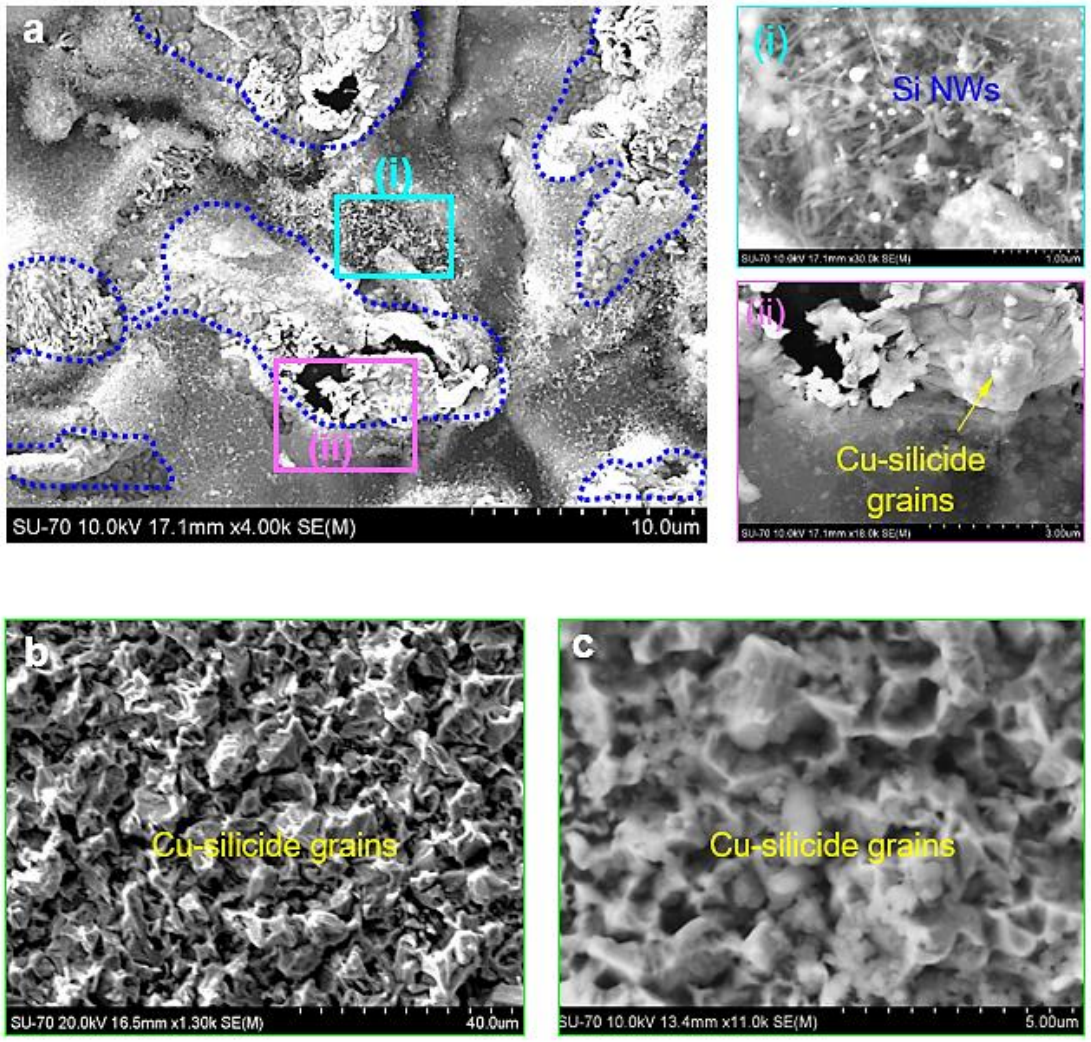

Figure S11 SEM images of (a) Si NWs and Cu-silicide grains (area in blue dotted-line) grown directly on Sn-coated planar Cu-foil and (b, c) Cu-silicide grains grown on the bare planar Cu-foil without any catalyst seeds.

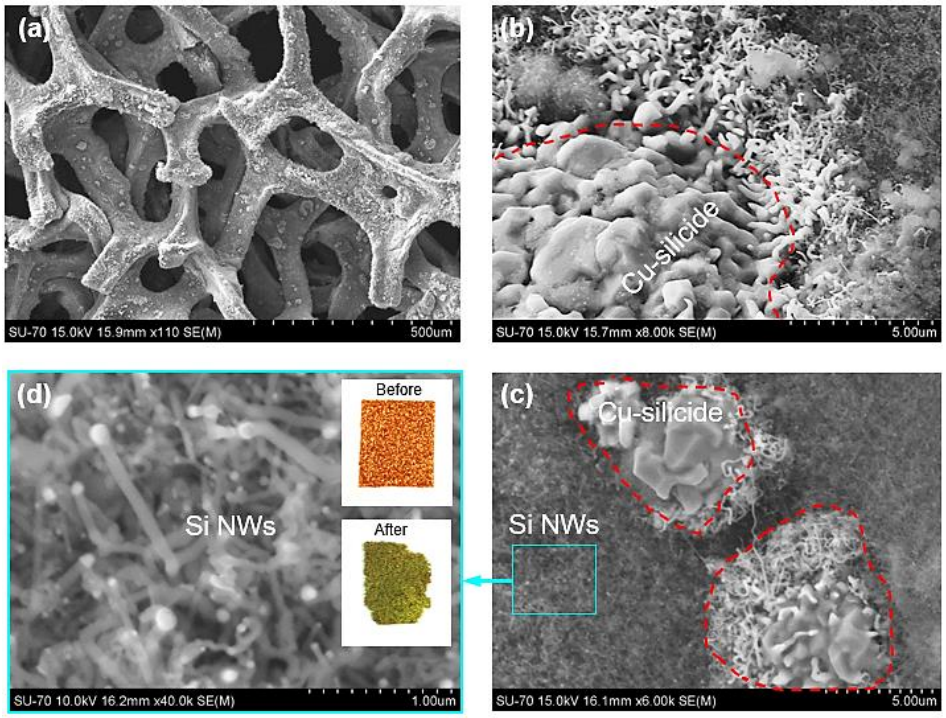

Figure S12 SEM images of Si NWs grown directly on commercial Cu-foam, showing islands of large grains of Cu/Si compounds. The inset images are the photographs of the Cu-foam before and after Si NWs growth.

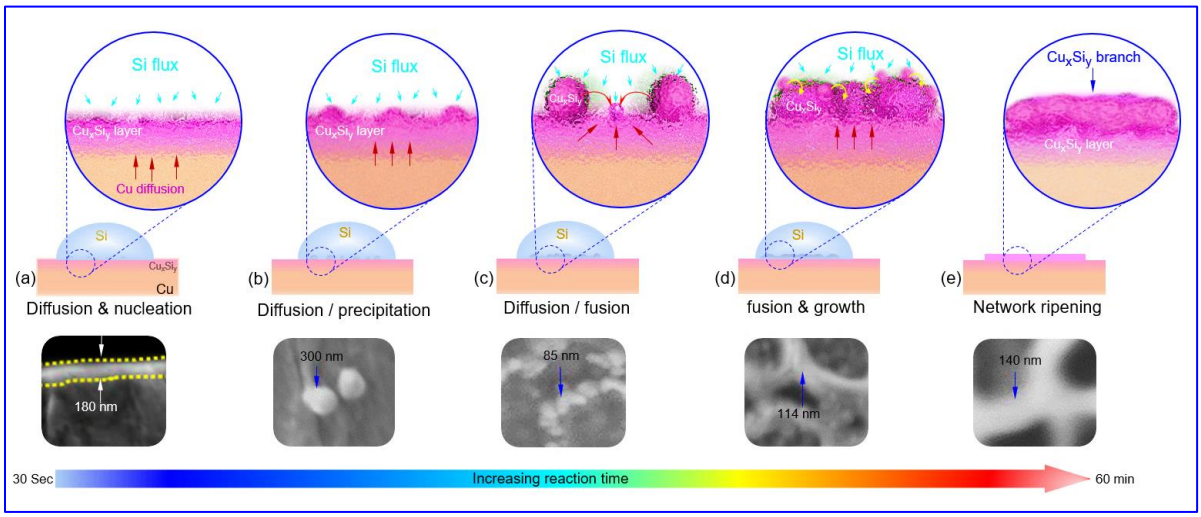

Figure S13 Structural evolution process of the 3D Cu_xSi_y NF and corresponding SEM images.

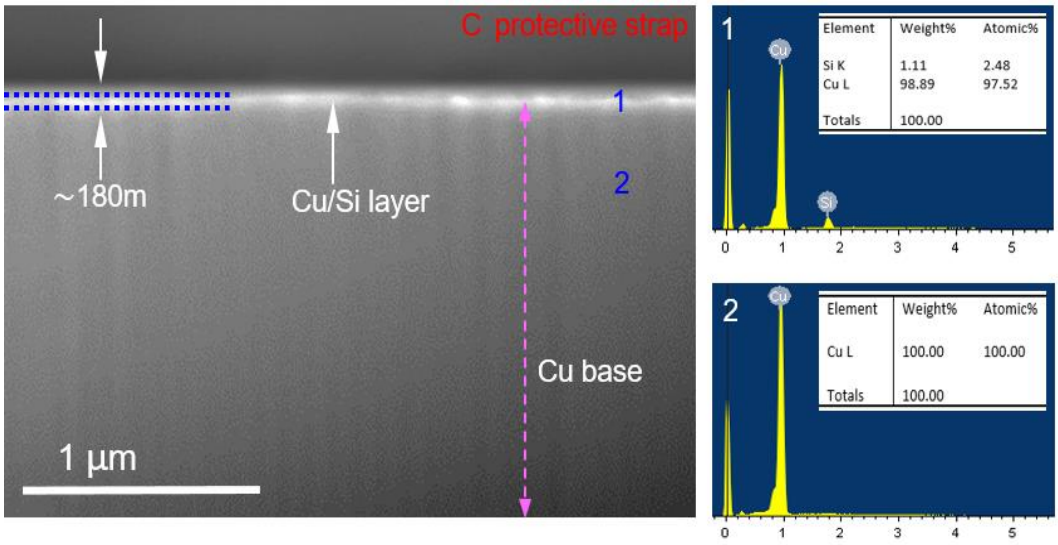

Figure S14 FIB-SEM cross-sectional images and corresponding EDX analysis showing the thin layer of Cu-rich silicide (~180 nm thick) formed within the first ~0.5 minutes.

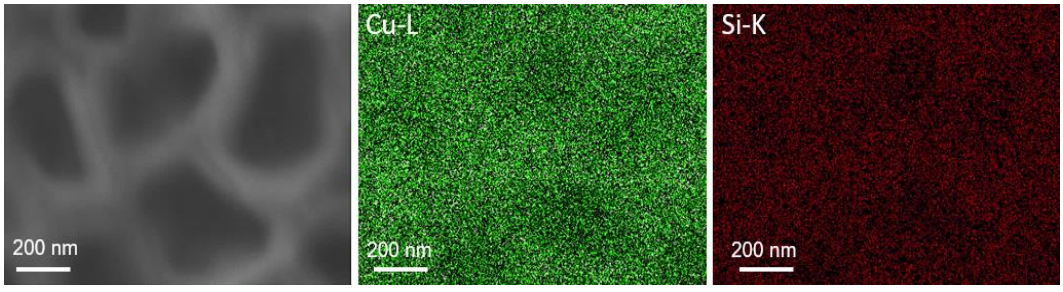

Figure S15 Mapping of elemental Cu and Si distribution in the 3D Cu_xSi_y NF.

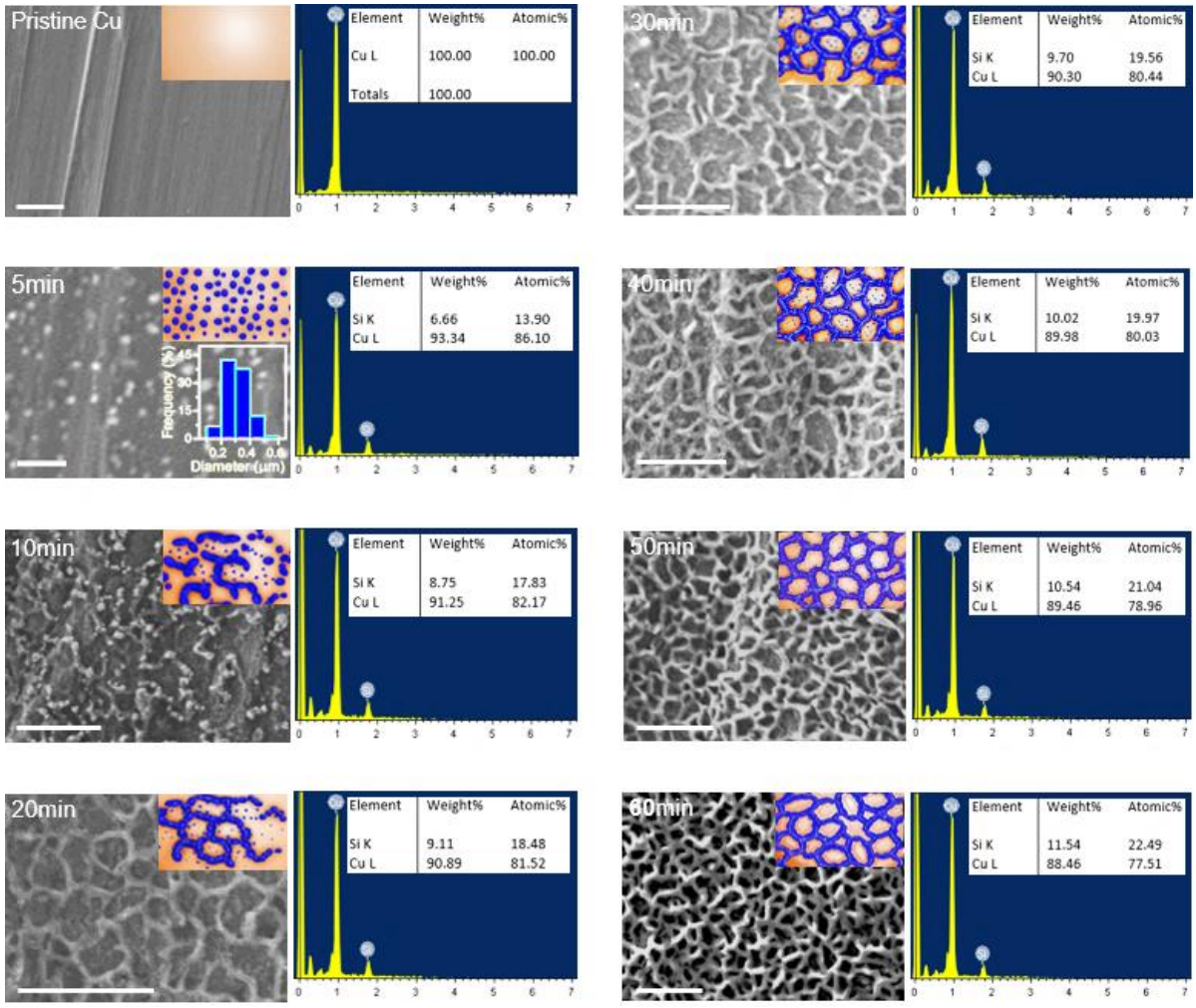

Figure S16 SEM images (scale: 2 μm) and corresponding EDX analysis of the discrete time point evolution of the 3D Cu_xSi_y network from the pristine Cu-foil upon reaction for ~5, ~10, ~20, ~30, ~40, ~50 and ~60 minutes. As clearly seen from the 10 – 40 minutes figures the sphere-like silicide nanoparticles continue to form along with the network branches and are gradually reduced to near disappearance by fusion into the branches at 50 – 60 minutes, thereby, consolidating the network branches. The Si to Cu atomic ratio also increases continuously as the network repines, indicating the availability of sufficient Si flux in the system to complete the reaction. Inset figures are the corresponding schematics depicting the gradual disappearance of the silicide nanoparticles and parallel proliferation of the network branches. The histogram in the @5 min image shows size distribution of the initially formed silicide nanoparticles.

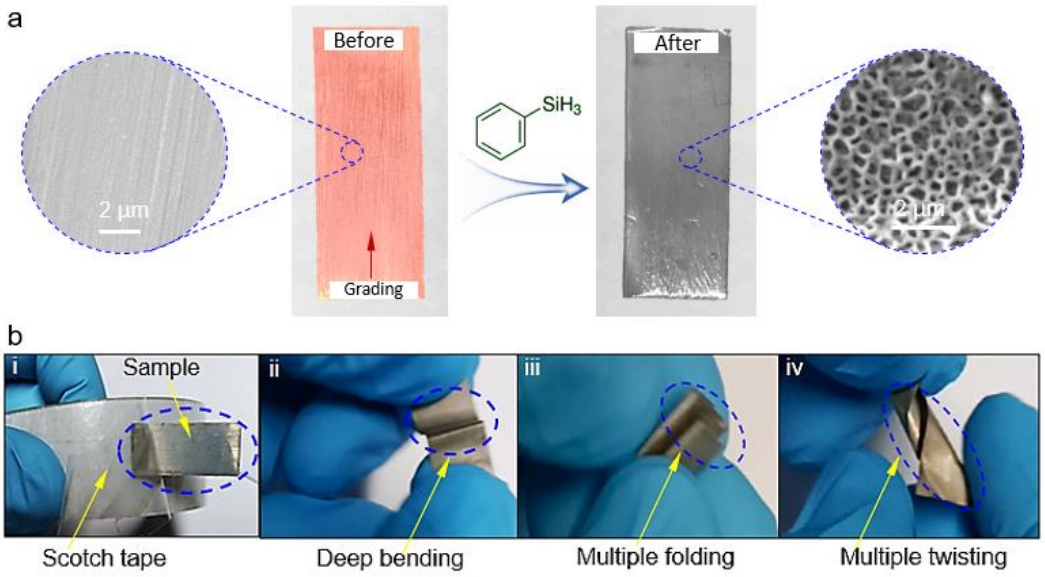

Figure S17 Photographs and corresponding SEM images of (a) pristine surface graded planar Cu-foil before and after the 3D Cu_xSi_y network formation (sample size: 3.0 cm^2) and (b) Photographs of the 3D Cu_xSi_y NF under (i) scotch tape peel off, (ii) deep bending, (iii) multiple folding and (iv) multiple twisting (see demonstrations in supplementary video1).

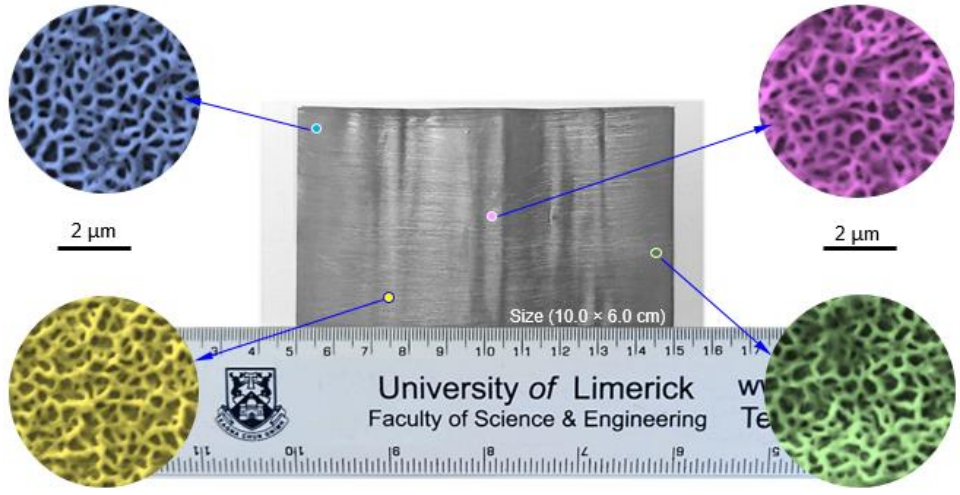

Figure S18 Photographs of a large-sized sample 3D Cu_xSi_y NF (60.0 cm^2) prepared under similar condition with SEM images taken from areas indicated by the dots in the photograph.

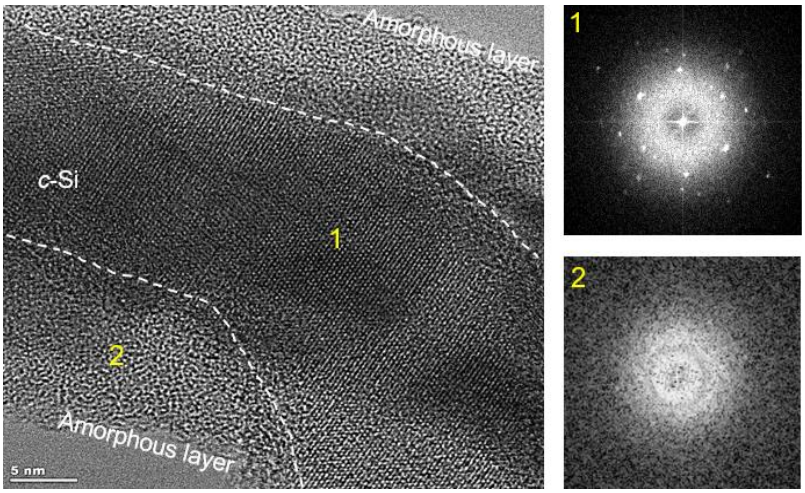

Figure S19 TEM image of Si NW showing amorphous layer deposition from excess Si flux and corresponding selected area fast Fourier diffractograms.

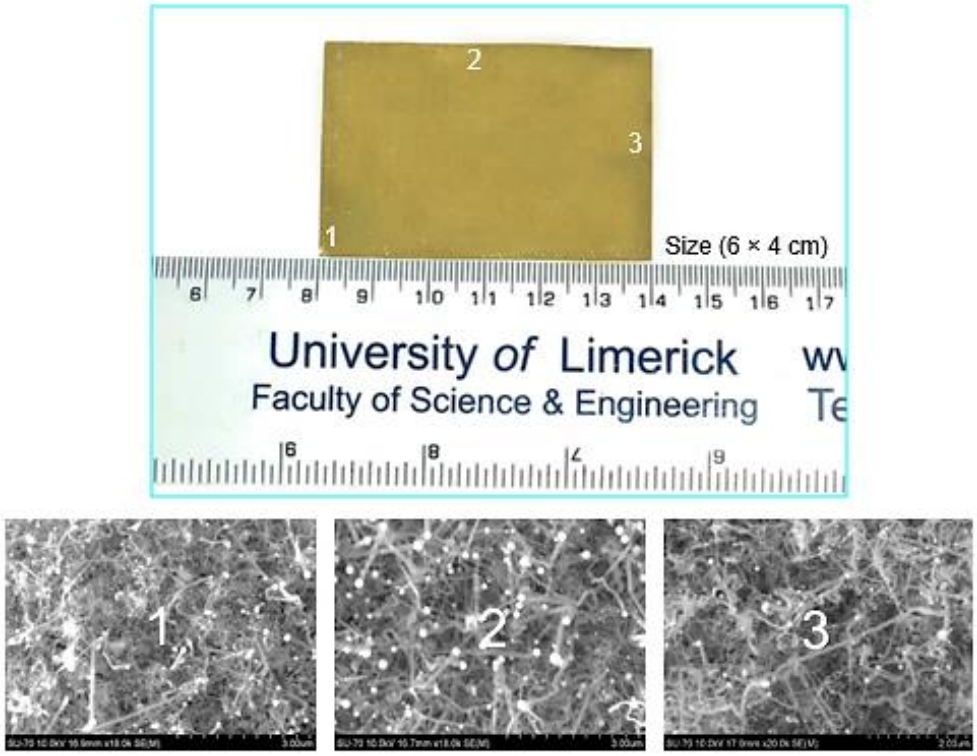

Figure S20 A photograph of large-sized sample of Sn-seeded Si NWs grown on the 3D Cu_xSi_y NF (sample area of 24 cm^2) and selected area SEM images.

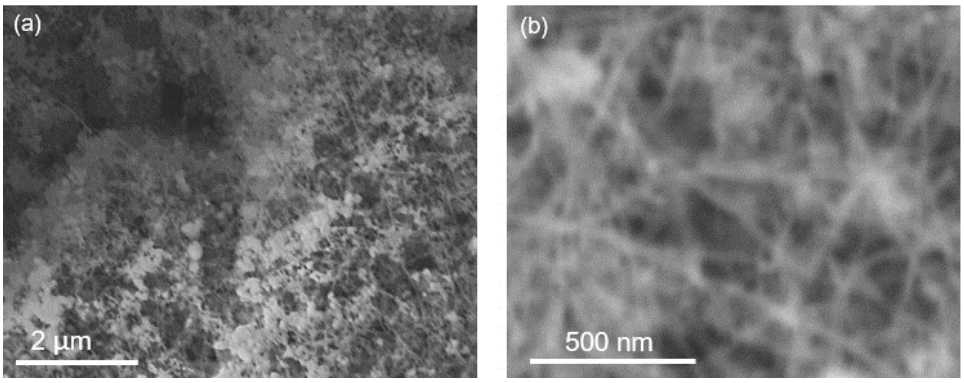

Figure S21 SEM images of Al-seeded Si NWs grown on the 3D Cu_xSi_y NF.

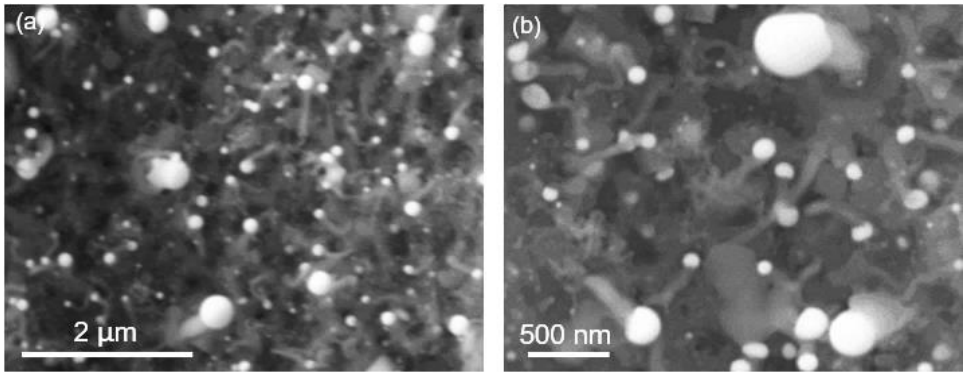

Figure S22 SEM images of Bi-seeded Si NWs grown on the 3D Cu_xSi_y NF.

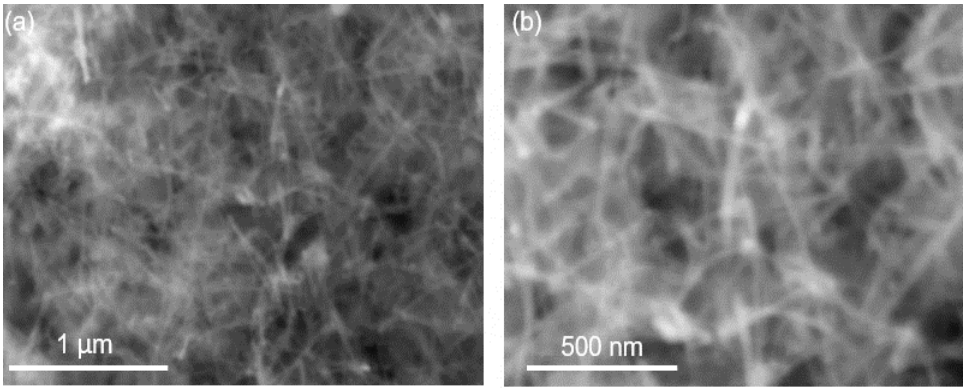

Figure S23 SEM images of Cu-seeded Si NWs grown on the 3D Cu_xSi_y NF.

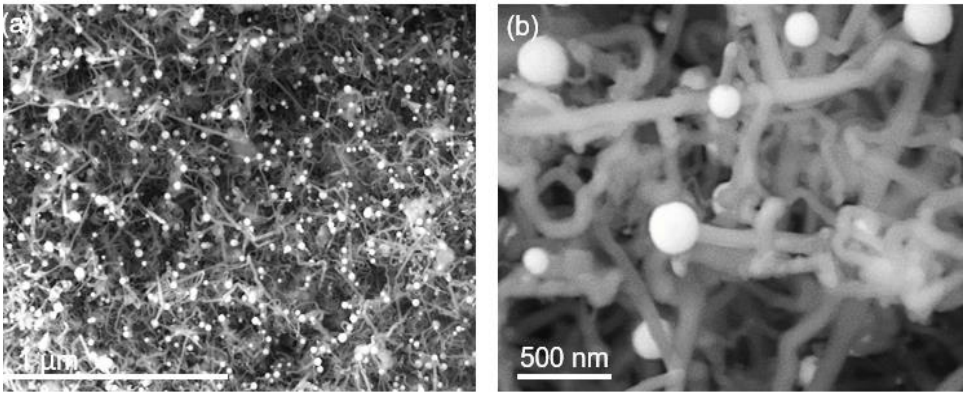

Figure S24 SEM images of In-seeded Si NWs grown on the 3D Cu_xSi_y NF.

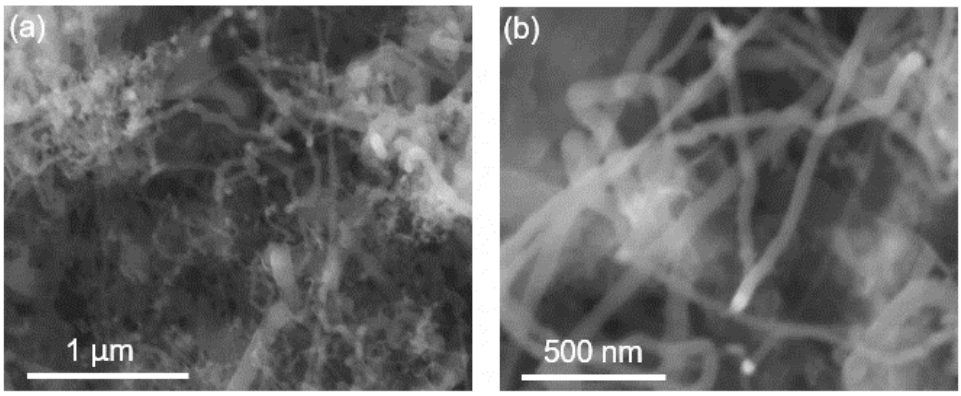

Figure S25 SEM images of Mn-seeded Si NWs grown on the 3D Cu_xSi_y NF.

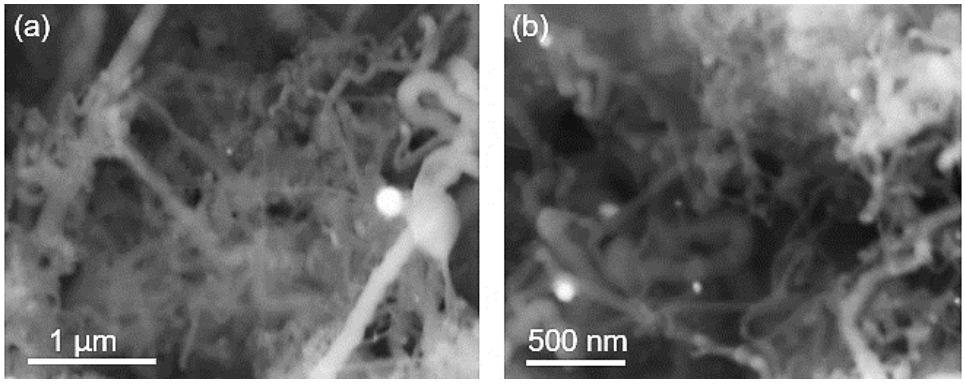

Figure S26 SEM images of Ni-seeded Si NWs grown on the 3D Cu_xSi_y NF.

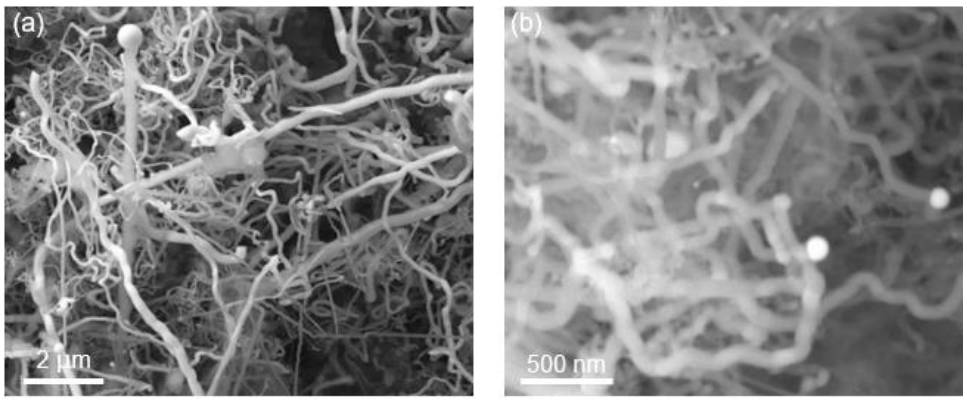

Figure S27 SEM images of Sb-seeded Si NWs grown on the 3D Cu_xSi_y NF.

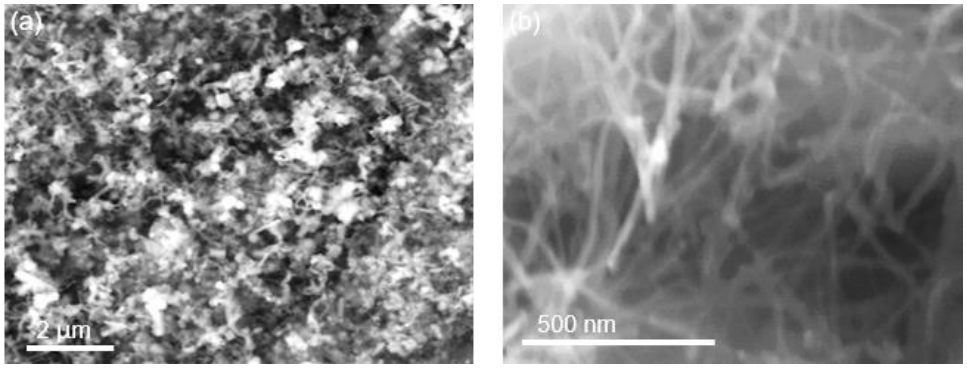

Figure S28 SEM images of Zn-seeded-Si NW grown on the 3D Cu_xSi_y NF.

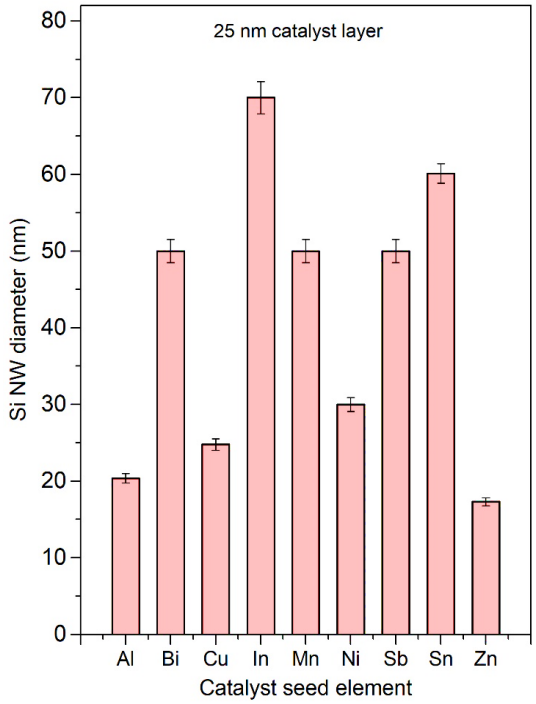

Figure S29 Average Si NW diameter by catalyst seed element. Differences in size may be influenced by the growth mechanism, e.g. VLS for Sn and VSS for Cu, etc.

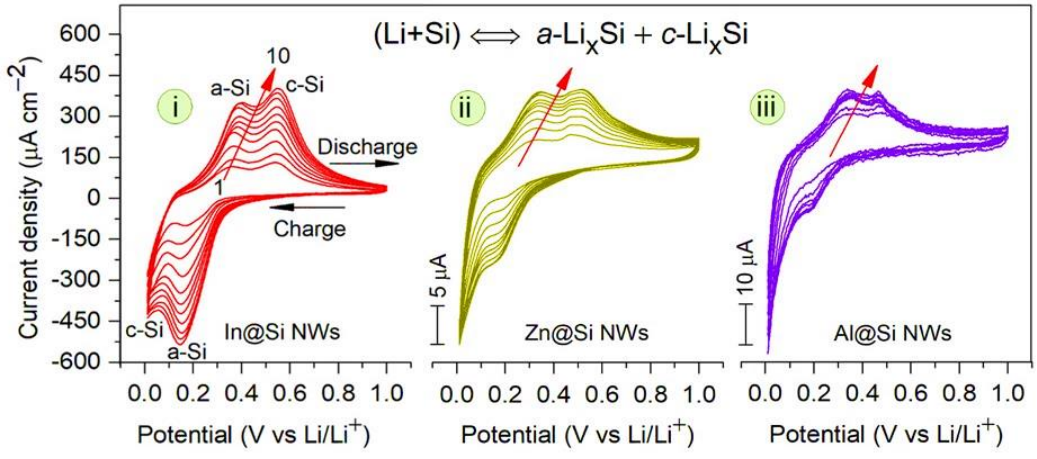

Figure S30 Cyclic voltammetry profiles of (i) In, (ii) Zn and (iii) Al seeded-Si NWs anodes.

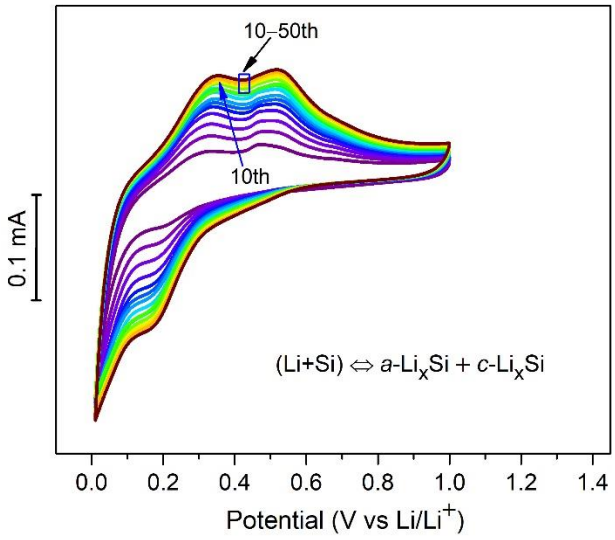

Figure S31 Cyclic voltammetry profiles of Sn-seeded Si NW, showing overlap beyond 10 cycles.

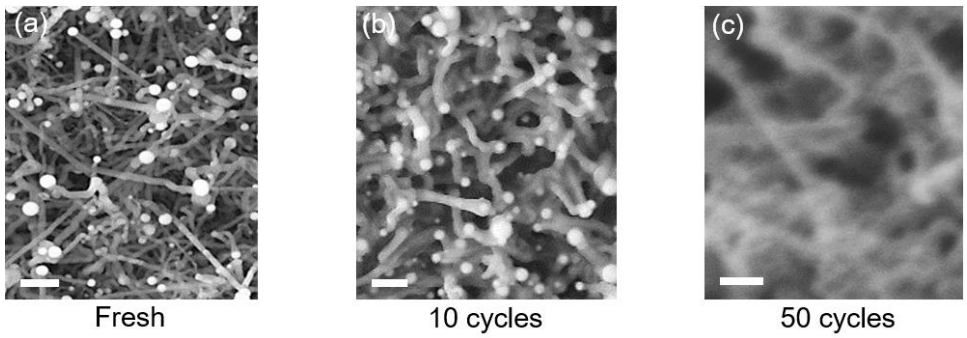

Figure S32 SEM images of Sn-seeded Si NWs anode (scale bars: 500 nm) before and after 10 and 50 cycles.

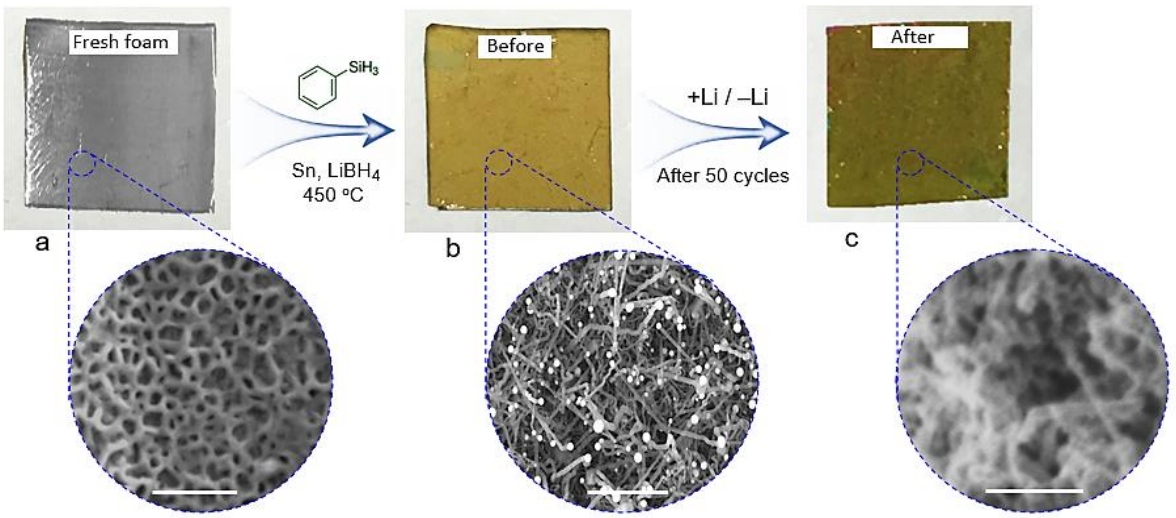

Figure 33 Photographs and corresponding FESEM images (scale bar: 2 μm) of (a) the bare 3D Cu_xSi_y NF and Sn-seeded Si NW@3D Cu_xSi_y NF anode (b) before and (b) after 50 cycles. The change in sample colour after reaction maybe influenced by electrochemical reactions, including electrolyte decomposition and/or oxidation.

Table S1. A comparison of the initial and final discharge capacities and percent retentivity relative to the cycling number and applied current for Si active anode.

Anode material	No. of Cycles	C-rate	Capacity (mAh g^{-1})		Retentive Capacity (%)	Reference
			Initial	Final		
Si NWs@Cu_xSi_y NF	550	C/10	2184	1655	75.8	***This work***
Mesoporous Si@Si/ Graphite	300	C/20	2834	1246	43.9	*Nano Lett.* **2018**, 18, 7060
Sn seeded Si NWs	250	C/5	1658	1333	80.3	*J. Power Sources* **2017**, 359, 601
Si NP cluster@ Si/graphite	300	C/20	3096	1388	44.8	*Nano Lett.* **2018**, 18, 7060
ALD TiO_2 coated Si NWs	100	C/10	3000	1600	53.3	*Phys. Chem. Chem. Phys.* **2013**, 15, 13646
Template assisted Si NWs	1100	C/2	3000	800	26.7	*Nano Lett.* **2013**, 13, 5740.
Core/shell Si NWs	100	C/5	1100	1000	90.9	*Nano Lett.* **2009**, 9, 491.
Carbon coated Si NWs	55	C/5	2000	1600	80.0	*Nano Lett.* **2009**, 9, 3370.
Interconnected Au@Si NWs	50	C/2	3500	2930	83.7	*Adv. Energy Mater*. **2011**, 1, 1154.
Cu-coated Si NWs	30	C/20	3700	2138	57.8	*J. Power Sources* **2011**, 196, 6657
Cu-Si-Al_2O_3 nanocables	100	C/10	1890	1560	82.5	*Adv. Mater*. **2011**, 23, 4415.
Si@nanoporous Ni	100	C/4	2444	2025	82.9	*J. Power Sources* **2012**, 213, 106.
Al_2O_3 coated Ni_xSi-Si core/shell NWs	120	C/20	3500	2750	78.6	*J. Mater. Chem.* **2012**, 22, 24618.
Double-walled Si nanotubes	900	C/5	1780	1352	75.9	*Nat. Nanotech.* **2012,** 7, 310.
Ni-silicide/Si core/shells	50	C/2	3733	2200	58.9	*CrystEngComm* **2013**, 15, 7298.
Si@3D foam	200	C/7	2500	1200	48.0	*J Mater. Chem. A* **2015**, 3, 10114.

Si NWs@ graphene interface	200	C/10	3360	2400	71.4	*Nano Lett.* **2015**, 15, 6658.
Si NWs@C on carbon fabric current collector	550	C/40	4000	2000	50.0	*Appl. Mater. Interfaces* **2017**, 9, 9551.
Cu/*a*-Si core/shell NWs	150	C/10	1730	1228	70.9	*Nanoscale* **2016**, 8, 2613.
Si NWs in ionic liquid electrolyte	500	C/2	2200	830	37.7	*ACS Nano* **2017**, 11, 5933.
Au-seeded Si NWs	10	C/20	3124	3000	96.0	*Nat. Nanotech.* **2008**, 3, 31.
Multi-shelled Si@ Cu MPs on 3D Cu	1500	C	1242	1080	86.9	*ACS Nano* **2018**, 12, 3587.
Si pomegranate	1000	C/20	2350	1,160	49.4	*Nat. Nanotech.* **2014**, 9, 187.
Si NW fabric	100	C/20	1484	804	54.1	*J. Am. Chem. Soc.* **2011**, 133, 20914

Note: For better and fair analysis of the capacity and percent retentivity, the ***C-rate*** and ***cycling number*** must be taken into consideration.

Table S2. A comparison of the initial discharge capacity and rententive areal capacity after cycling for binder-free and traditional slurry based Si active anodes.

Anode material	Mass loading (mg cm^{-2})	No. of Cycles	Gravimetric Capacity (mAh g^{-1})	Ret. Areal Capacity (mAh cm^{-2})	Reference
Si NWs@Cu_xSi_y NF	1.20	550	2183	2.00	***This work***
Multilayer Si/CNT	0.07	50	2913	0.40	*Energy Environ. Sci*. **2014**, *7*, 655.
Ge@a-Si NWs	0.41	150	2066	0.85	*ACS Appl. Mater. Interfaces* **2019**, 11, 19372.
$Si_{1-x}Ge_x$ thin films	0.05	60	2121	0.11	*ACS Nano* **2013**, 7, 2249.
Si-Ge heterostructure NWs	0.10	400	1644	0.16	*Nano Lett*. **2018**, 18, 5569.
AMPSi@C	1.40	100	2843	1.90	*Nat. Commun*, **2019**, 10, 1447.
Si@Porous Cu	0.10	60	910	0.75	*Solid State Ionics* **2016**, *288*, 204.
TCG-Si	1.90	200	1390	2.40	*Nano Lett*. **2015**, 15, 6222.
Si NW–CNT	0.50	35	2400	1.60	*Adv. Energy Mater*. **2012**, *2*, 87.
Multicomponent Si-based anodes	3.75	1000	1000	1.80	*Energy Environ. Sci*. **2015**, 8, 2075.
Si/Carbon/CMC	1.50	100	1000	1.40	*Chem. Mater*. **2010**, 22, 1229
5wt%-Gr–Si	0.10	200	2400	0.90	*Nat. Commun*. **2015**, *6*, 7393.
Si NP–Si NW network	0.30	50	1600	1.90	*Chem. Commun*. 2011, 47, 367.
Si pomegranate	2.34	200	2350	2.10	*Nat. Nanotech*. **2014**, 9, 187
Si -PEDOT:PSS-CNT	2.00	100	2209	1.80	*Adv. Energy Mater*. **2014**, 4, 1400207.

GF/Si NWs	0.30	100	2423	0.35	*RSC Advances* **2016**, 6, 1678
Cu/Si/Ge NW	1.20	100	2373	1.26	*Energy. Environ. Sci*. **2018**, 11, 669.
Nano-Si/SnO_2 core–shell	n/a	50	1000	n/a	*J. Mater. Chem.* A, **2013**, 1 , 3733.
Si-Ge Alloy Nanotubes	3.0	100	1146	3.44	*Angew. Chem. Int. Ed.* **2016**, 55, 7427.
Si/Ge Double Layer nanotubes	n/a	50	1546	1.20	*ACS Nano* **2012**, 6, 303.
N-PSi@C	23.0	200	3188	1.50 [FC]	*ACS Nano* **2019**, 13, 2307.

Note: For better and fair analysis, the ***mass loading*** and ***cycling number*** must be taken into consideration. (FC) indicates full cell